Epilepsy & Behavior 48 (2015) 21–28

Contents lists available at ScienceDirect

Epilepsy & Behavior

journal homepage: www.elsevier.com/locate/yebeh

Cortical feature analysis and machine learning improves detection of "MRI-negative" focal cortical dysplasia

Bilal Ahmed [a], Carla E. Brodley [a], Karen E. Blackmon [b], Ruben Kuzniecky [b], Gilad Barash [a], Chad Carlson [b], Brian T. Quinn [b], Werner Doyle [b], Jacqueline French [b], Orrin Devinsky [b], Thomas Thesen [b,c,*]

[a] Department of Computer Science, Tufts University, Medford, MA, USA
[b] Comprehensive Epilepsy Center, Department of Neurology, School of Medicine, New York University, New York, USA
[c] Department of Radiology, School of Medicine, New York University, New York, USA

ARTICLE INFO

Article history:
Received 17 March 2015
Revised 21 April 2015
Accepted 22 April 2015
Available online 31 May 2015

Keywords:
Epilepsy
Focal cortical dysplasia
Machine learning
Structural MRI

ABSTRACT

Focal cortical dysplasia (FCD) is the most common cause of pediatric epilepsy and the third most common lesion in adults with treatment-resistant epilepsy. Advances in MRI have revolutionized the diagnosis of FCD, resulting in higher success rates for resective epilepsy surgery. However, many patients with histologically confirmed FCD have normal presurgical MRI studies ('MRI-negative'), making presurgical diagnosis difficult. The purpose of this study was to test whether a novel MRI postprocessing method successfully detects histopathologically verified FCD in a sample of patients without visually appreciable lesions. We applied an automated quantitative morphometry approach which computed five surface-based MRI features and combined them in a machine learning model to classify lesional and nonlesional vertices. Accuracy was defined by classifying contiguous vertices as "lesional" when they fell within the surgical resection region. Our multivariate method correctly detected the lesion in 6 of 7 MRI-*positive* patients, which is comparable with the detection rates that have been reported in univariate vertex-based morphometry studies. More significantly, in patients that were MRI-negative, machine learning correctly identified 14 out of 24 FCD lesions (58%). This was achieved after separating abnormal thickness and thinness into distinct classifiers, as well as separating sulcal and gyral regions. Results demonstrate that MRI-negative images contain sufficient information to aid in the in vivo detection of visually elusive FCD lesions.

1. Introduction

Despite advances in pharmacotherapy for the treatment of epilepsy, approximately one-third of patients remain to have seizures refractory to medications [1]. For patients with treatment-resistant epilepsy (TRE), the best option for achieving seizure freedom is often surgical resection. In patients where a focal seizure onset is identified through a comprehensive presurgical evaluation, surgical resection results in seizure freedom rates ranging from 30 to 80% [2]. Despite a growing number of studies demonstrating that surgery is effective for patients with focal TRE, it remains underutilized [3]. Patients who lack an MRI-visible lesion are less likely to be referred to a specialized epilepsy center by neurologists [4], and many epilepsy specialists are reluctant to recommend surgery without a well-defined lesion.

Focal cortical dysplasia (FCD), a malformation of cortical development (MCD), is the most common epileptogenic lesion in children and the third most common in adults with TRE [5,6]. Typical MRI features of FCD include cortical thickening or thinning, blurring of the gray–white matter junction, increased signal intensities on FLAIR and/or T2-weighted images, a transmantle stripe of T2 hyperintensity, and localized brain atrophy [7]. However, 45% of histologically confirmed FCD lesions go undetected by routine visual inspection of the MRI [8], which may be in part due to the anatomical complexity of the cortex. This makes FCD the most common histopathological finding in patients with no visible lesion on MRI [9,10].

The feasibility of utilizing quantitative MRI methods for detecting visually apparent (i.e., MRI-positive) FCD lesions has been established using voxel-based morphometry [11–14]. Cortical surface-based methods have been combined in a multivariate approach with high accuracy in classifying small, visually subtle FCD lesions [15,16]. Surface-based measures of cortical thickness, gray and white matter blurring, and sulcal depth contribute the most predictive weight in multivariate linear discriminant analyses, with cortical thickness offering the greatest specificity to the primary lesion [16]. This approach provides class II evidence that automated machine learning of MRI patterns can accurately identify FCD lesions that were radiologically diagnosed as MRI-negative, although these lesions were ultimately found to be visually apparent and manually traceable when texture-based maps were provided to expert reviewers.

Here, we present a quantitative morphometry approach that combines surface-based MRI processing methods with machine learning

* Corresponding author at: Comprehensive Epilepsy Center, Department of Neurology, New York University, 223 34th Street, New York, NY 10016, USA.
E-mail address: thomas.thesen@med.nyu.edu (T. Thesen).

http://dx.doi.org/10.1016/j.yebeh.2015.04.055
1525-5050/

algorithms to detect FCD lesions in patients classified as MRI-negative following conventional radiological analysis of scans acquired through a standard epilepsy protocol. The novelty of our approach is that it utilizes specific strategies to model the biological features of FCD lesions. For example, we train separate classifiers on abnormally thick versus abnormally thin lesional regions to model these features separately, which can vary by FCD lesion subtype [7]. Additionally, we train separate classifiers for the gyral wall, sulcus, and crown to optimize detection of bottom-of-the-sulcus lesions [17].

2. Materials and methods

2.1. Participants

Participants were selected from a large registry of patients with epilepsy treated at the New York University School of Medicine Comprehensive Epilepsy Center who signed consent for a research MRI scanning protocol. Criteria for inclusion in this study included the following: (1) completion of a high resolution T1-weighted MRI scan, (2) surgical resection to treat focal epilepsy, and (3) diagnosis of FCD on neuropathological examination of the resected tissue. These selection criteria resulted in a sample of 31 patients with FCD. Demographic- and seizure-related information for these participants is provided in Table 1.

In addition, MRI scans using identical imaging parameters from a total of 62 neurotypical controls were acquired (31 females; ages 17–65; mean age = 33; SD = 12.5). Exclusion criteria for the control group included any history of psychiatric or neurological disorders.

2.2. Image acquisition

2.2.1. Imaging for research

Imaging for the research protocol was performed at the New York University Center for Brain Imaging on a Siemens Allegra 3T scanner. Image acquisitions included a conventional 3-plane localizer and a T1-weighted volume pulse sequence (TE = 3.25 ms, TR = 2530 ms, TI = 1100 ms, flip angle = 7-degree field of view (FOV) = 256 mm, matrix = 256 × 256, vertex size = 1 × 1 × 1.3 mm, scan time: 8:07 min). Acquisition parameters were optimized for increased gray/white matter image contrast. The T1-weighted image was reoriented into a common space, roughly similar to alignment based on the AC–PC line. Images were corrected for nonlinear warping caused by non-uniform fields created by the gradient coils.

2.2.2. Clinical imaging

Clinical imaging sequences for radiological review were acquired at the NYU Department of Radiology on a 3-Tesla Siemens scanner. Clinical sequences were variable across patients but commonly included high-resolution T1-weighted MPRAGE (magnetization-prepared rapid gradient echo) images, T2-weighted images (axial and coronal, varying slice thickness from 1 to 3 mm), and fluid-attenuated inversion recovery (FLAIR) images (2–6 mm slice thickness). The research T1-weighted MPRAGE images used in our analyses were included in the set of images reviewed by the clinical radiology team. Conventional visual analysis of the clinical scans resulted in an MRI diagnosis of FCD in 7 patients (MRI-positive) and a "normal" report in 24 patients (MRI-negative). The higher number of MRI-negative patients in this sample may be due to a tendency for patients with more complex, MRI-negative epilepsy to be referred to our level 4 epilepsy treatment center.

2.3. Surface reconstruction

The research MRI sequences were processed using the FreeSurfer software package (http://surfer.nmr.mgh.harvard.edu/), which performs automated tissue segmentation to recreate 3D representations of the cortical surfaces from structural MRI scans [18]. Briefly, after skull stripping, the method [18] involves (i) segmentation of the white matter, (ii) tessellation of the gray/white matter boundary, (iii) inflation of the folded surface, and (iv) correction of topological defects. Once the surface was reconstructed, it was further refined by classifying all white matter vertices in the MRI volume to create the gray/white matter boundary. The gray/white matter junction was delineated up to submillimeter accuracy by further refining the white matter surface. After refining the gray/white matter junction, the pial surface was located by deforming the surface outward. Each segmentation and reconstruction underwent manual inspection and editing, when necessary. However, the high image quality and gray–white contrast in the initial images resulted in minimal editing requirements for both patient and control scans. Surface reconstruction was followed by a registration process that involved morphing the reconstructed surface to an average spherical representation that accurately matched sulcal and gyral features across individual subjects while minimizing metric distortion [19].

Table 1
Demographic- and seizure-related information of both MRI-positive and MRI-negative patients.

Patient	Location	Age (years)	Sex	Seizure onset age (years)	Seizure frequency (per year)	Engel class
MRI-positive subjects						
NY49	R temporal	39	M	20	6	1
NY53	L frontal	18	F	10	44	1
NY123	L parietal	14	M	7	730	2
NY143	R frontal	38	F	4	1248	1
NY156	L temporal	20	M	7	182	2
NY187	L temporal	45	F	5	14	1
NY194	R temporal and R occipital	40	F	7	9	1
Mean		31		8.6	319	
MRI-negative subjects						
NY46	R temporal	41	M	3	52	1
NY51	L frontal, L insular, and L temporal	14	F	1	365	4
NY67	R temporal	27	M	13	1825	1
NY68	L temporal	26	M	15	12	2
NY72	R temporal	46	M	74	2	2
NY98	L frontal and L insular	20	M	14	42	4
NY116	R temporal	30	M	22	84	1
NY130	L temporal	22	M	14	3	3
NY148	L temporal	37	M	35	3	2
NY149	R frontal	32	F	11	1460	1
NY169	R temporal	26	M	3	1277	1
NY171	R temporal	26	F	19	5	4
NY177	L temporal	38	F	19	5	3
NY207	R temporal	30	F	25	1	1
NY212	L temporal	37	M	21	166	1
NY226	R temp	40	F	5	8	1
NY241	L temporal	21	M	11	27	1
NY255	R temporal	20	F	15	48	–[a]
NY259	L temporal	26	F	9	288	2
NY294	R temporal	51	F	1	12	1
NY297	R temporal	51	F	8	52	1
NY299	R temporal	28	F	13	37	2
NY312	L temporal	43	F	6	24	1
NY322	R frontal, R insular, and R temporal	24	F	9	12	1
Mean		31		15.3	242	

M = male and F = female.
[a] Patient lost during follow-up.

2.4. Morphometric feature extraction

Five cortical features were computed at each vertex. These included (i) cortical thickness, (ii) gray/white matter contrast, (iii) sulcal depth, (iv) mean curvature, and (v) Jacobian distortion.

(i) *Cortical thickness* was assessed at each location by using an average of two measurements: (a) the shortest distance from the white matter surface to the pial surface and (b) the shortest distance from the pial surface at each point to the white matter surface.

(ii) *Gray/white matter contrast* (GWC) was estimated by calculating the nonnormalized T1-weighted image intensity contrast at 0.5 mm above and below the gray/white interface with trilinear interpolation of the images. The range of GWC values was [−1, 0], with values near zero indicating a higher degree of blurring of the gray/white boundary.

(iii) *Sulcal depth* was estimated by calculating the dot product of the movement vectors with the surface normal [20] and results in the calculation of the depth/height of each point above the average surface. The values of sulcal depth lie in the range [−2, 2], with lower values indicating a location in the sulcus whereas higher values indicate a location on the gyral crown. We used the sulcal depth measure to stratify the classification into sulcus, wall, and gyrus because these areas differ in cortical thickness and gray–white contrast distribution [21] and there is evidence that FCD occurs predominantly in sulcal regions [22,17].

(iv) *Curvature* is measured as 1 / r, where r is the radius of an inscribed circle and mean curvature represents the average of two principal curvatures with a unit of 1/mm [23]. Mean curvature quantifies the sharpness of cortical folding at the gyral crown or within the sulcus and can be used to assess the folding of small secondary and tertiary folds in the cortical surface.

(v) In the registration process, as defined above, each subject's gyral and sulcal features are aligned by warping the entire brain to a spherical average surface (i.e., the 'standard brain'). During this process, each vertex is subjected to a nonlinear spherical transform. *Jacobian distortion* measures the magnitude of the nonlinear transform at each vertex needed to warp each vertex on the subject's brain to a target vertex on the average surface. It is a measure of global brain deformation and has also been applied at the vertex level in various neurological disorders [24].

2.5. Normalization of parameters

In preparing the data for the machine learning classifier, the cortical features from each patient are z-score normalized using the mean and standard deviation calculated from the control population, on a vertex-by-vertex basis.

2.6. Lesion and resection tracing

For MRI-positive patients, an expert on epileptogenic malformations on cortical development and who is board-certified in neurology and neurophysiology (RK), reviewed the clinical MRI report and manually traced the outer regions of the visible lesions on the morphometric T1-weighted 3D volume scan based on the lesional areas identified in the initial clinical report or during surgical conference. When available, the visual detection was aided by T2-weighted FLAIR images from the standard clinical epilepsy MRI protocol. For MRI-negative patients, the postoperative T1-weighted image (with the resection area removed) was rigid-body coregistered to the (intact) preoperative T1-weighted image using FLIRT [25]. The brain resection area was manually traced on the postsurgical MRI scan by a trained technician blinded to patient diagnosis and reviewed by a board-certified neurologist. For both lesion and resection tracings, the manual masks in the vertex space were subsequently projected onto the cortical surface by assigning each vertex to the nearest surface vertex. Because the surface has subvertex resolution, a morphological closing operation was used to fill in any unlabeled vertices.

2.7. Univariate (z-score) analysis

In order to compare the machine learning approach to a univariate approach that uses surface-based morphometry [26], a z-score statistic was calculated for cortical thickness which was found to be the most informative feature according to Thesen et al. [26] at each vertex between a single patient and the control group. Cluster thresholding at $p < .05$ was applied to correct for multiple comparisons [27]. Images were thresholded at $z = 2.1$ ($p = .035$) [26].

2.8. Machine learning classification

Machine learning algorithms are ideally suited for dysplasia detection in that they can incorporate multiple quantitative MRI measures, making maximum use of all relevant data available. The goal of the machine learning classification model was to accurately differentiate contiguous clusters of lesional vertices from nonlesional vertices in a single patient. Accuracy was defined by classifying contiguous vertices as "lesional" when they fell within the manually traced lesion or resection region for MRI-positive and MRI-negative patients, respectively, and "nonlesional" when they fell outside of these regions.

Designing an appropriate classification scheme for detecting FCD under these constraints has three important challenges. First, class label noise arises from subjectivity in delineating the lesion zone (either a manually traced MRI-visible zone or resection-defined zone). Second, the anatomic complexity and heterogeneity in folded cortical tissue reduce the ability to discern lesional tissue from the normal cortex, which is one of the reasons why a large number of lesions remain elusive to human perception in routine radiological evaluation [28]. Third, class imbalance [29] results from a ratio of substantially fewer lesional to nonlesional vertices for a particular patient. The class imbalance problem is further compounded by the higher availability of healthy control data compared to patient data. We address each of these challenges in turn.

2.8.1. Addressing class label noise

Optimizing classifiers for detecting FCD lesions relies on accurately labeling vertices as "lesional" or "nonlesional" in the training data. Class label noise can arise from errors in human decision-making and subjectivity, in addition to the anatomical complexity of the brain itself. For example, labeling "lesional" vertices in MRI-positive cases involves subjective tracing of the FCD lesion. Moreover, in the absence of an MRI-visible lesion, lesional vertices are delineated by the extent of the tissue removed in surgery, which may include a gradation from abnormal to normal tissue. From a supervised machine learning perspective, treating all the resected vertices in the case of MRI-negative patients as being lesional introduces substantial false positives into the training data, which can have adverse effects on classifier accuracy [30].

The fact that the resection zones in MRI-negative patients include both lesional tissue and nonlesional tissue is problematic for training classifiers. Hong et al. [16] address this problem by utilizing a preprocessing step that not only includes the generation of texture maps [31,32] but also requires human expertise and intervention to visually identify and trace lesions. In our approach, we used cortical thickness to reduce the impact of false-positive label noise. Cortical thickness is the most prominent feature on T1-weighted imaging in FCD [7,26,33]. We, therefore, trained the classifier on the vertices inside the resection zone that showed the highest degree of thickness abnormality both in terms of thickening and thinning.

Normal tissue classification was performed on data from control subjects in order to control false negatives in the labeled data that can arise because the lifetime seizure burden of a given patient can lead to cortical abnormalities outside the seizure onset zone [34–37] or the possibility of additional nonepileptogenic dysplastic lesions [38]. In addition, patients who are suffering from epilepsy due to developmental factors may have additional lesions that either are not epileptogenic or have latent epileptogenicity. Based on these considerations, we chose not to include nonlesional vertices from the subjects as negative instances in our training data.

2.8.2. Reducing cortical complexity

Anatomical complexity of the cortical convolution may account for why many lesions remain undetected in radiological MRI evaluations. The folding of the cortex varies across individuals, and it can hinder the visibility of subtle FCD lesions that may be hidden deep within the folds. Recent studies have shown that subtle FCD lesions occur with higher frequency at the bottom of the sulcus. Given these observations, we designed a stratified classification scheme composed of different classifiers that were trained separately for sulcal, wall, and gyral regions. We separated the data into three nonoverlapping levels where (i) sulcal depth in the range $[-2, -1]$ represents vertices that are part of the sulcus, (ii) $[1, 2]$ represents vertices residing on the gyrus, and (iii) the vertices in-between (i.e., with a sulcal depth of $[-1, 1]$) were labeled as wall vertices. Partitioning the vertices into these three groups meant that we needed to calculate the two thresholds for mitigating label noise per sulcal level, which resulted in a total of six distinct thresholds (i.e., 1. thin/sulcus, 2. thick/sulcus, 3. thin/gyrus, 4. thick/gyrus, 5. thin/wall, and 6. thick/wall). In other words, for each sulcus level X, we trained two separate classifiers, which differed in how the training data for lesional vertices were collected. Specifically, one classifier was based on vertices of sulcal depth X and thinning values less than our threshold "τ-thin" whereas the other classifier was based on vertices of sulcal depth X with cortical thickening greater than our threshold "τ-thick". Note that although we used cortical thickness to reduce the lesion area, our classifiers employed all four cortical metrics to represent each vertex (i.e., cortical thickness, GWC, cortical curvature, and Jacobian distortion).

2.8.3. Addressing class imbalance

This problem arises out of having substantially fewer vertices labeled as "lesional" than vertices labeled as "nonlesional." Such an imbalance in training data can result in classifiers that are biased towards the majority class [29]. To address this issue, we used a "bagging" approach [39]. We construct a set of "base-level" classifiers, each trained using logistic regression, using an iterative-reweighted least squares (IRLS) algorithm [40]. Each base-level classifier is trained on all the minority class instances (lesional vertices) and an equal-sized random sample of majority class instances (nonlesional instances). A "bag" of ten "base-level" classifiers was trained for each of the resulting six subsets of vertices. To classify a vertex as lesional or nonlesional, we first used its sulcal depth to choose the two correct bags of classifiers (e.g., if the sulcal depth was "sulcus", we use the "thin/sulcus" and "thick/sulcus" classifiers). Next, each of the ten base-level classifiers was applied for each bag. The final classification was obtained by a majority vote of their predictions. The overall training and testing phases of the proposed classification scheme are shown in Figs. 1A and B, respectively.

2.9. Experimental method

A leave-one-out cross-validation (LOOCV) strategy was used to test the performance of the classifier on unseen data. In each run, we left out a single subject from the data and trained a classifier on vertices belonging to all the remaining subjects and the controls. The output of each logistic regression classifier within the bag is the probability that the given input vertex belongs to the positive (lesional) class. To convert this probability into a class label, we defined a threshold $\rho = 0.95$ for the output values such that the vertices that have a predicted probability above ρ were deemed lesional and those that fall below ρ were considered normal. After classifying each vertex of the test subject, the results were postprocessed [26] to remove spurious detections by defining the detected cluster as a set of contiguous lesional vertices having a surface area greater than or equal to 50 mm^2, an approach similar to [41] where the threshold was determined as the area of the largest cluster detected by the classifier in the control population.

To determine detection values, patients were regarded as true positives if any of the remaining clusters partially or completely overlapped with the lesion/resection area. Outside clusters were considered false positives. It should be kept in mind that the resulting detection outside the lesion/resection zone may actually represent other malformations in the cortex that either have escaped visual inspection or were not part of the seizure onset zone. Thus, the statistics provided here represent a *lower bound* on actual classifier performance.

2.9.1. Performance evaluation metrics

We use three metrics to quantify and contrast the performance of our classification scheme with the baseline univariate approach. These include the true positive rate (TPR), the false positive rate (FPR), and the Dice coefficient (DC) [42]. The DC is a set similarity metric that is a special case of the kappa statistic [43]. It is commonly used to measure the accuracy of segmentation in medical images when ground truth is available [44,45]. We use DC to measure the overlap between the final detected clusters (after postprocessing) and the resection or expert-traced lesion for a test patient.

Let, the resection/lesion zone be represented by a binary vector $M_{\text{label}} \in \{0,1\}$, and let $M_{\text{pred}} \in \{0,1\}$ be the binary vector representing the detection results. The metrics are then defined as follows:

$$\text{TPR}(M_{\text{label}}, M_{\text{pred}}) = \frac{|M_{\text{pred}} \cap M_{\text{label}}|}{|M_{\text{label}}|} \tag{1}$$

$$\text{FPR}(M_{\text{pred}}, M_{\text{label}}) = \frac{|M_{\text{pred}} \cap \overline{M}_{\text{label}}|}{|\overline{M}_{\text{label}}|} \tag{2}$$

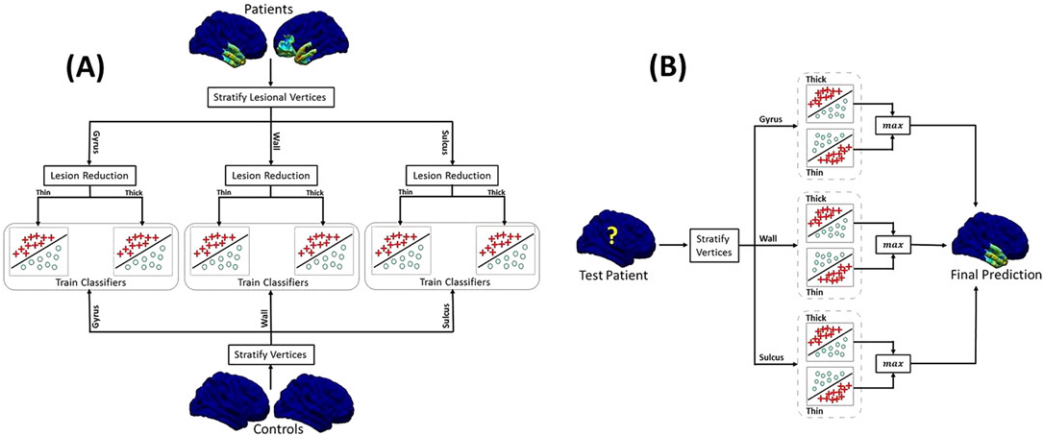

Fig. 1. Different steps involved in the (A) training and (B) test phases of the proposed classification scheme. Note that the lesion reduction step is applied only to the training patients. For a test subject, we calculate two labels per vertex: one from each thick/thin classifier. The final label of the vertex is calculated as the maximum of both predicted labels.

$$DC(M_{pred}, M_{label}) = \frac{2|M_{pred} \cap M_{label}|}{|M_{pred}| + |M_{label}|} \quad (3)$$

where $|M|$ represents the first norm of the binary vector and, in our case, translates to the number of vertices marked as lesional and $\overline{M}$ represents an inverted mask, such that the original 0 values are replaced with 1 and vice versa.

3. Results

In this section, we review the performance of our proposed classification scheme and contrast it with the baseline z-score-based method. We also provide empirical evidence to support our design decisions, i.e., classifier stratification, mask reduction, and bagging.

3.1. Overview of the detection results

For MRI-positive patients, both the z-score and machine learning approaches were found to perform identically and accurately detected lesions in 6 out of 7 patients, yielding an 86% detection rate (Table 2). Machine learning correctly identified a significantly larger proportion ($t(7) = 3.3$, $p < 0.05$) of the lesional area (mean = 20.14%) compared to the z-score approach (mean = 16.03%) as quantified by the TPR. However, the differences in the DC values were found to be not statistically significant. The false-positive rate was significantly lower for the z-score approach (mean = 1.4%) compared to the machine learning approach (mean = 2.4%; $t(7) = 5.1$, $p < .01$) (see Table 2). Fig. 2A shows an example of a detected lesion in an MRI-positive patient. Detailed results for both approaches are listed in Table 2.

For patients with MRI-negative lesions, the machine learning approach significantly outperformed the z-score-based method. The z-score-based method correctly detected lesions in 9 out of the 24 patients (37%), whereas the machine learning approach correctly detected clusters inside the resection zone for 14 patients (58%) (see Table 2). Fig. 2B shows an example of a detected lesion in an MRI-negative subject. The overall true-positive rate was significantly higher ($t(23) = 3.04$, $p < 0.01$) in the machine learning approach (mean = 2.5%) compared to the z-score approach (mean = 1.1%). The DC values for the machine learning approach (mean = 3.68%) were also significantly superior ($t(23) = 3.04$, $p < 0.01$) to the baseline (mean = 1.87%). However, the false-positive rate was also significantly higher ($t(23) = 5.65$, $p < .001$) in the machine learning approach (mean = 1.0%) compared to the z-score approach (0.6%). Detailed results are shown in Table 2.

3.2. Sensitivity analysis of design decisions

In order to determine whether correcting for cortical complexity by stratifying classifiers by sulcal depth results in improved detection rates, we reran the training phase in the leave-one-out cross-validation without this correction (note that we retain bagging and mask reduction). As depicted in Tables 3 and 4 (compare the ML column to column "A"), the true-positive rate dropped from 20.1% to 12.9% in the MRI-positive group and lesion detection dropped from 58% to 33% in the MRI-negative group. This suggests that different feature combinations might be more prevalent in specific regions (e.g., sulcus, gyrus, and wall), which is consistent with the observation of region-specific dysplasia subtypes (e.g., bottom-of-the-sulcus dysplasia).

In order to correct for the class label noise problem, we employed a strategy to reduce vertices labeled as "lesional" to those that were significantly thicker or thinner than "nonlesional" vertices. We tested the improvement in detection rates when utilizing this strategy by rerunning our analysis without mask reduction (note that we retained stratification and bagging for this experiment). The results are again depicted in Tables 3 and 4 (compare the ML column to column "B") and show a drop in detection rates for both the MRI-positive group (from 6/7 to 3/7) and the MRI-negative group (from 14/24 to 3/24 detections). This indicates that class label noise is a significant issue for both groups that can be corrected by utilizing a mask reduction strategy with a separate threshold for cortical thickening and cortical thinning.

Our last experiments examined the impact of bagging on the results (we eliminated bagging and retained stratification and mask reduction). We see from Tables 3 and 4 that eliminating bagging resulted in the most substantial drop in performance; the TPR of the MRI-positive group dropped from 20.1% to 2.1%, and for the MRI-negative group, the detection rate dropped from 14/24 to 0/24. In other words, failing to correct for the class imbalance problem resulted in zero detection of MRI-negative FCD lesions. This strongly supports the use of such bagging and stratified classifiers in future machine learning models for FCD detection. Fig. 3 summarizes our results and contrasts the rate of detection for MRI-negative patients under different variations in the design of the machine learning approach.

Table 2
Detection results for both MRI-positive and MRI-negative subjects.

Subject ID	z-Score			ML		
	TPR	FPR	DC	TPR	FPR	DC
MRI-positive						
NY49	11.85	1.00	19.92	24.76	2.27	34.58
NY53	20.28	2.60	29.60	27.72	4.46	35.42
NY123	29.80	3.68	27.61	31.33	4.50	26.36
NY143	16.38	0.60	12.28	20.03	2.00	5.81
NY156	26.12	1.20	38.69	25.65	2.11	36.14
NY187	–	0.50	–	–	0.90	–
NY194	7.79	0.14	14.00	11.48	0.58	18.18
Mean	16.03	1.40	20.30	20.14	2.41	22.36
MRI-negative						
NY46	–	0.34	–	0.95	0.74	1.78
NY51	2.86	1.00	5.11	4.15	1.02	7.24
NY67	4.35	0.26	8.13	8.30	0.65	14.45
NY68	0.09	1.33	0.14	0.12	1.69	0.15
NY72	–	–	–	0.55	0.25	1.07
NY98	–	0.33	–	–	0.81	–
NY116	–	–	–	–	0.39	–
NY130	–	0.16	–	–	0.25	–
NY148	–	0.10	–	–	0.12	–
NY149	–	0.84	–	–	1.68	–
NY169	–	1.02	–	9.41	1.98	8.97
NY171	2.45	1.00	2.93	2.94	1.80	2.57
NY177	1.88	0.14	3.59	3.20	0.32	5.80
NY207	–	0.05	–	–	0.60	–
NY212	–	1.01	–	–	1.60	–
NY226	–	0.50	–	1.09	0.60	1.88
NY241	–	0.33	–	–	0.40	–
NY255	3.23	0.42	6.01	6.18	1.30	10.30
NY259	–	0.50	–	–	0.58	–
NY294	–	0.50	–	–	1.40	–
NY297	2.98	0.14	5.64	7.98	0.56	13.30
NY299	–	3.13	–	3.30	4.86	4.32
NY312	6.10	0.50	10.05	9.04	0.97	12.83
NY322	1.74	0.31	3.25	2.02	0.49	3.66
Mean	1.07	0.58	1.87	2.47	1.04	3.68

For each subject, the true-positive rate (TPR) and false-positive rate (FPR) are calculated as the percentage of lesional vertices correctly labeled and the percentage of nonlesional vertices incorrectly labeled, respectively. The Dice coefficient (DC) is also shown as a percentage to quantify the overlap between the detected clusters and the resection on the cortical surface.

4. Discussion

Our results demonstrate that surface-based morphometry, coupled with a multivariate classification scheme that is adapted for FCD lesion data, can successfully detect epileptogenic FCD lesions on MRIs that were previously interpreted as normal by neuroradiologists. This approach correctly identified epileptogenic regions in 58% of MRI-negative patients compared to 37% when using univariate statistics. A separate analysis showed that while the best detectors of FCD lesions

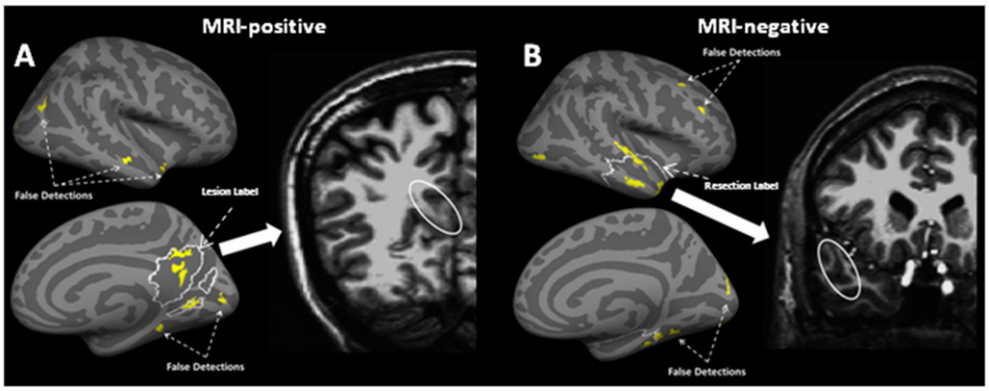

Fig. 2. Detection results for the ML-based approach for (A) an MRI-positive and (B) an MRI-negative patient. The inflated lateral and medial cortical surfaces show the original expert-traced lesion (A) or the resection zone (B) as the regions outlined by the white solid curve. The significant lesional clusters discovered by the ML-based approach are shown in yellow. The MRI slice on the right shows the abnormal area corresponding to the clusters discovered inside the lesion/resection on the actual brain volume.

were cortical thickness and GWC, features commonly used in the visual diagnosis of FCD, measures of cortical complexity, such as curvature and Jacobian distortion, also contributed strongly to lesion detection. This finding suggests that MRI images contain ample information about focal epileptogenic lesions but do so to a degree and in a complexity that may not be appreciable by visual inspection alone.

Malformations of cortical development are the third most frequent disease entity associated with TRE, and FCD is the underlying pathology in 75% of these cases [46]. Resection of FCD tissue is critical to seizure control; therefore, it is an important target for MRI evaluation during presurgical assessment. The presurgical detection of a lesion informs intracranial electrode placement and provides a valuable target that, when surgically resected, can lead to a substantial improvement in postsurgical outcome [47,48]. Indeed, surgical success in patients with neocortical epilepsy and a concordant MRI lesion is drastically improved (66%) compared to cases without lesions (29%) [49].

The application of machine learning algorithms to the detection of FCD lesions resulted in a unique set of challenges that are specific to this clinical population, requiring innovative solutions. The existence of these challenges and the improvement in classification when solutions were implemented offer a unique perspective on the biological complexity of focal cortical dysplasia. One such challenge was the presence of abnormal vertices outside of the histopathologically confirmed focal dysplastic region. Although these are considered to be statistical false positives, alternative explanations must also be considered, such as the following: (1) the presence of a dysplastic cortex outside of the seizure onset zone may or may not have latent epileptogenic potential [38] and/or (2) the burden of intractable seizures on brain structure could result in subtle abnormalities (e.g., atrophy and gliosis) that may be difficult to distinguish from developmental aberrations [34–37,50]. Both of these possibilities could impact postsurgical outcomes and are thus worth further exploration. For example, magnetoencephalography or intracranial electroencephalography could be used to determine whether there is abnormal electrophysiology in these "false-positive" regions. Tracking postsurgical outcomes could determine whether a greater extent of "extralesional" abnormalities is associated with suboptimal postsurgical seizure control or functional outcomes.

Table 3
A comparison of detection results using the z-score-based method and the ML method only for MRI-positive subjects with different variations in the design of the ML approach.

Patient	z-Score		ML		(A)		(B)		(C)	
	TPR	FPR	TPR	FPR	TPR	FPR	TPR	FPR	TPR	FPR
NY49	11.8	1.0	24.8	2.3	8.7	0.6	–	–	0.6	–
NY53	20.3	2.6	27.7	4.5	23.5	4.2	10.6	1.2	4.3	0.2
NY123	29.8	3.7	31.3	4.5	31.4	4.6	25.2	1.2	7.4	0.1
NY143	16.4	0.6	20.0	2.0	–	0.4	–	–	–	0.1
NY156	26.1	1.2	25.7	2.1	26.4	1.8	20.1	0.4	2.1	–
NY187	–	0.5	–	0.9	–	0.6	–	0.4	–	–
NY194	7.8	0.1	11.5	0.6	–	–	–	–	–	–
Mean (%)	16.0	1.4	20.1	2.4	12.9	1.7	8.0	0.5	2.1	0.1

(A) No stratification along the sulcal values, (B) stratifies the data based on the sulcal depth values but does not reduce the lesion mask, and (C) uses stratification and lesion reduction, but it does not use bagging. The TPR and FPR are measured as a percentage.

An additional challenge for machine learning algorithms is the heterogeneity of pathological and MRI features in FCD. For example, FCD lesions might contain small diameter cells that may result in an abnormally thin cortex on MRI [51] or large dysmorphic cells that may result in an abnormally thick cortex on MRI [7]. We observed improved classification rates when we stratified labeling of "lesion" vertices in the lesion zone/resection zone based on separate thresholds for cortical thickening and thinning. Additionally, specific regions of the cortical architecture may be more vulnerable to dysplastic pathology. Focal cortical dysplasia lesions occur with higher frequency at the bottom of the sulcus, potentially reflecting different "micromechanic" tensions that enhance pathophysiological vulnerability in the sulcal bottom [22]. We observed improvement when we stratified classifiers trained separately for sulcal, wall, and gyral regions. The improvement in our model after implementing such solutions suggests that similar stratification strategies should be employed in future FCD lesion detection efforts.

The resection zones of MRI-negative patients include both lesional tissue and nonlesional tissue; therefore, the resection zone cannot be treated as a gold standard for training classifiers. Hong et al. [16] utilize a mask reduction step in which texture maps [31,32] are used to manually trace the lesion for MRI-negative patients that have type II FCD. This preprocessing not only entails the generation of texture maps but also requires specific human expertise to identify lesions. In the proposed approach, we use cortical measures to reduce the resection mask, such that the resected regions that are not significantly different from the regions outside the resection zone are not used for training the classifier. We hypothesize that this approach will accurately classify FCD lesions in a sample of patients with verified MRI-negative FCD lesions.

The methodological approach used in the current study to improve lesion detection of MRI-negative images has a number of significant advantages. First, it works with most existing scanners and sequences and does not require advanced imaging technologies. Second, as we learn more about FCD, stratification of larger data sets into distinct FCD subtypes [52] can be incorporated into future training sets to help the system learn specific subtype features and potentially classify FCD by subtype. Third, such a method can be fully automated and thus, with minimal effort, can augment visual inspection by yielding targets for closer evaluation by neuroradiologists. This latter point is important, given the fact that the visual detection of FCD on MRI varies

Table 4
A comparison of detection results using the z-score-based method and the ML method only for MRI-negative subjects with different variations in the design of the ML approach.

Patient	z-Score		ML		(A)		(B)		(C)	
	Detected	FPR	Detected	FPR	Detected	FPR	Detected	FPR	Detected	FPR
NY46	N	0.34	Y	0.74	N	–	N	–	N	–
NY51	Y	1.00	Y	1.02	Y	0.95	Y	0.30	N	–
NY67	Y	0.30	Y	0.65	Y	0.19	N	–	N	–
NY68	Y	1.33	Y	1.69	Y	1.56	Y	0.81	N	–
NY72	N	–	Y	0.25	N	–	N	–	N	–
NY98	N	0.33	N	0.81	N	0.56	N	–	N	–
NY116	N	–	N	0.39	N	–	N	–	N	–
NY130	N	0.16	N	0.25	N	0.16	N	–	N	–
NY148	N	0.10	N	0.12	N	0.10	N	–	N	–
NY149	N	0.84	N	1.68	N	0.18	N	–	N	0.06
NY169	N	1.02	Y	1.98	N	0.09	N	–	N	–
NY171	Y	1.00	Y	1.80	Y	–	N	–	N	–
NY177	Y	0.14	Y	0.32	Y	0.30	N	–	N	–
NY207	N	0.05	N	0.60	N	–	N	–	N	–
NY212	N	1.01	N	1.60	N	1.13	N	0.53	N	0.06
NY226	N	0.50	Y	0.60	N	0.46	N	0.20	N	–
NY241	N	0.33	N	0.40	N	0.35	N	0.08	N	–
NY255	Y	0.42	Y	1.30	Y	0.08	N	–	N	–
NY259	N	0.50	N	0.58	N	0.50	N	0.17	N	–
NY294	N	0.50	N	1.40	N	0.20	N	–	N	–
NY297	Y	0.14	Y	0.56	Y	–	N	–	N	–
NY299	N	3.13	Y	4.86	N	0.30	N	–	N	–
NY312	Y	0.50	Y	0.97	Y	0.73	Y	–	N	–
NY322	Y	0.31	Y	0.49	Y	0.12	N	–	N	–
Mean (%)	9/24 (38%)	0.58	14/24 (58%)	1.04	8/24 (33%)	0.33	3/24 (12%)	0.09	0/24 (0%)	0.005

(A) No stratification along the sulcal values, (B) stratifies the data based on the sulcal depth values but does not reduce the lesion mask, and (C) uses stratification and lesion reduction, but it does not use bagging. FPR is given as a percentage.

widely among raters, and is highly dependent on the experience of the evaluator.

4.1. Limitations

In the current study, training data in MRI-negative cases were derived from resection areas that were defined by intracranial electrophysiology. Focal cortical dysplasia pathology was present in the resection area in all patients; however, nonlesional tissue may have also been resected. We reduced this problem by applying a mask reduction step, and this increased performance. In future research studies, this step can be improved by accurately coregistering the pathological sample with the MRI, allowing the matching of pathological and MRI slices.

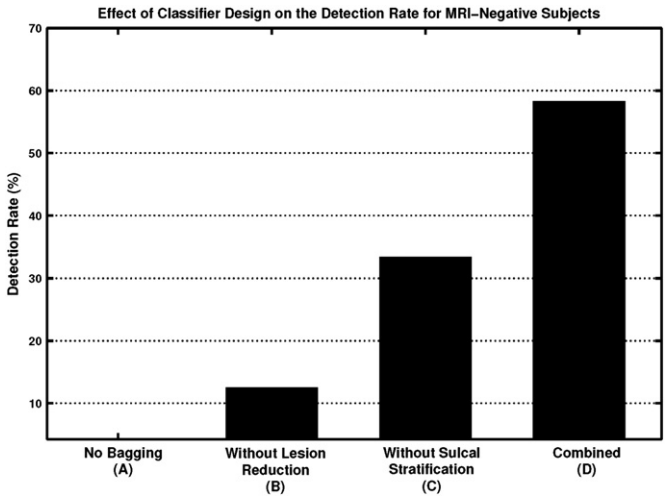

Fig. 3. A comparison of detection results in MRI-negative subjects with different variations in the design of the ML approach, including (A) without bagging (cf. Section 2.8.3) but with sulcal stratification and lesion reduction, (B) without lesion reduction (cf. Section 2.8.1) but with bagging and sulcal stratification, (C) without stratification (cf. Section 2.8.2) but with bagging and lesion reduction, and (D) using all including bagging, lesion reduction, and sulcal stratification.

In addition, our sample of MRI-negative patients was disproportionately higher than MRI-positive patients, which may not reflect the proportions seen at other neurological clinics. This likely represents a bias in patient referrals to our level 4 epilepsy center, which offers intensive neurodiagnostic monitoring for patients with treatment-resistant epilepsy that is difficult to localize. Our results offer a potential advancement of neurodiagnostic tools for this more challenging population. However, the case–control methods that we utilize in our approach require a large healthy control MRI data set with identical scanning parameters as those of the patient and thus cannot be readily applied in any clinical center. Further investigations with combined data sets from different scanners and institutions are needed to create methods for making these analyses feasible with different scanning sequences across centers. Finally, automated detection and classification of lesions should not replace careful visual analysis of a trained expert. Rather, the quantitative approach can be used to supplement visual analysis by highlighting areas with a high lesional probability. These results should always be interpreted in the context of all available patient information collected during presurgical evaluation.

5. Conclusion

In summary, we have demonstrated that a quantitative morphometric method using surface-based brain modeling, combined with machine learning algorithms and novel strategies to deal with the complexity of cortical malformations, results in improved detection of FCD. Improved detection of neocortical structural lesions is likely to increase the number of patient referrals to specialized tertiary epilepsy centers for surgical consideration and, in many cases, may decrease the delay between initial diagnosis and surgery. This has significant implications for improved seizure and cognitive outcomes in patients with FCD and concomitant epilepsy.

Acknowledgments

We would like to thank John Brumm, Omar Khan, and Christine Chao for help with data processing and Rachel Jurd for comments. This research is supported by FACES—Finding a Cure for Epilepsy and Seizures (TT) and the Epilepsy Foundation (KEB, BA, and CC).

Conflict of interest

The authors declare no competing financial interests.

References

[1] Kwan P, Brodie MJ. Early identification of refractory epilepsy. N Engl J Med 2000; 342(5):314–9.
[2] Tellez-Zenteno JF, Dhar R, Wiebe S. Long-term seizure outcomes following epilepsy surgery: a systematic review and meta-analysis. Brain 2005;128(Pt 5):1188–98.
[3] Benbadis SR, Heriaud L, Tatum WO, Vale FL. Epilepsy surgery, delays and referral patterns—are all your epilepsy patients controlled? Seizure 2003;12(3):167–70.
[4] Hakimi AS, Spanaki MV, Schuh LA, Smith BJ, Schultz L. A survey of neurologists' views on epilepsy surgery and medically refractory epilepsy. Epilepsy Behav 2008; 13(1):96–101.
[5] Kuzniecky RI, Barkovich AJ. Malformations of cortical development and epilepsy. Brain Dev 2001;23(1):2–11.
[6] Lerner JT, Salamon N, Hauptman JS, Velasco TR, Hemb M, Wu JY, et al. Assessment and surgical outcomes for mild type I and severe type II cortical dysplasia: a critical review and the UCLA experience. Epilepsia 2009;50(6):1310–35.
[7] Muhlebner AR, Coras R, Kobow CK, Feucht M, Czech T, Stefan H, et al. Neuropathologic measurements in focal cortical dysplasias: validation of the ILAE 2011 classification system and diagnostic implications for MRI. Acta Neuropathol 2012;123(2): 259–72.
[8] Wang ZI, Alexopoulos AV, Jones SE, Jaisani Z, Najm IM, Prayson RA. The pathology of magnetic-resonance-imaging-negative epilepsy. Mod Pathol Off J U S Can Acad Pathol Inc 2013;26:1051–8.
[9] Alarcon G, Valentin G, Watt C, Selway RP, Lacruz ME, Elwes RD, et al. Is it worth pursuing surgery for epilepsy in patients with normal neuroimaging? J Neurol Neurosurg Psychiatry 2006;77(4):474–80.
[10] Wetjen NM, Marsh WR, Meyer FB, Cascino GD, So E, Britton JW, et al. Intracranial electroencephalography seizure onset patterns and surgical outcomes in nonlesional extratemporal epilepsy. J Neurosurg 2009;110(6):1147–52.
[11] Kassubek J, Huppertz HJ, Spreer J, Schulze-Bonhage A. Detection and localization of focal cortical dysplasia by vertex-based 3-D MRI analysis. Epilepsia 2002;43(6): 596–602.
[12] Colliot O, Bernasconi N, Khalili N, Antel SB, Naessens V, Bernasconi A. Individual vertex-based analysis of gray matter in focal cortical dysplasia. Neuroimage 2006; 29(1):162–71.
[13] Bonilha L, Montenegro MA, Rorden C, Castellano G, Guerreiro MM, Cendes F, et al. Vertex-based morphometry reveals excess gray matter concentration in patients with focal cortical dysplasia. Epilepsia 2006;47(5):908–15.
[14] Pail M, Mareček R, Hermanová M, Slaná B, Tyrlíková I, Kuba R, et al. The role of voxel-based morphometry in the detection of cortical dysplasia within the temporal pole in patients with intractable mesial temporal lobe epilepsy. Epilepsia 2012; 53(6):1004–12.
[15] Besson P, Bernasconi N, Colliot O, Evans A, Bernasconi A. Surface-based texture and morphological analysis detects subtle cortical dysplasia. Med Image Comput Comput Assist Interv 2008;11(Pt 1):645–52.
[16] Hong SJ, Kim H, Schrader D, Bernasconi N, Bernhardt BC, Bernasconi A. Automated detection of cortical dysplasia type II in MRI-negative epilepsy. Neurology 2014; 83(1):48–55.
[17] Hofman PA, Fitt GJ, Harvey AS, Kuzniecky RI, Jackson G. Bottom-of-sulcus dysplasia: imaging features. AJR Am J Roentgenol 2011;196(4):881–5.
[18] Dale AM, Fischl B, Sereno MI. Cortical surface-based analysis. I. Segmentation and surface reconstruction. Neuroimage 1999;9(2):179–94.
[19] Fischl B, Dale AM. Measuring the thickness of the human cerebral cortex from magnetic resonance images. Proc Natl Acad Sci U S A 2000;97(20):11050–5.
[20] Fischl B, Sereno MI, Dale AM. Cortical surface-based analysis. II: inflation, flattening, and a surface-based coordinate system. Neuroimage 1999;9(2):195–207.
[21] Blackmon K, Halgren E, Barr WB, Carlson C, Devinsky O, DuBois J, et al. Individual differences in verbal abilities associated with regional blurring of the left gray and white matter boundary. J Neurosci 2011;31(43):15257–63.
[22] Besson P, Andermann F, Dubeau F, Bernasconi A. Small focal cortical dysplasia lesions are located at the bottom of a deep sulcus. Brain 2008;131(Pt 12):3246–55.
[23] Pienaar R, Fischl B, Caviness B, Makris N, Grant PE. A methodology for analyzing curvature in the developing brain from preterm to adult. Int J Imaging Syst Technol 2008;18(1):42–68.
[24] Good CD, Ashburner J, Frackowiak RS. Computational neuroanatomy: new perspectives for neuroradiology. Rev Neurol 2001;157(8–9 Pt1):797–806.
[25] Jenkinson M, Bannister P, Brady M, Smith S. Improved optimisation for the robust and accurate linear registration and motion correction of brain images. Neuroimage 2002;17(2):825–41.
[26] Thesen T, Quinn BT, Carlson C, Devinsky O, DuBois J, McDonald CR, et al. Detection of epileptogenic cortical malformations with surface-based MRI morphometry. PLoS One 2011;6(2):e16430.
[27] Hagler Jr DJ, Saygin AP, Sereno MI. Smoothing and cluster thresholding for cortical surface-based group analysis of fMRI data. Neuroimage 2006;33(4):1093–103.
[28] Tassi L, Colombo N, Garbelli R, Francione S, Lo Russo G, Mai R, et al. Focal cortical dysplasia: neuropathological subtypes, EEG, neuroimaging and surgical outcome. Brain 2002;125(8):1719–32.
[29] Japkowicz N, Stephen S. The class imbalance problem: a systematic study. Intell Data Anal 2002;6(5):429–49.
[30] Brodley CE, Friedl M. Identifying mislabeled training data. J AI Res 1999;11:131–67.
[31] Bernasconi A, Antel SB, Collins DL, Bernasconi N, Olivier A, Dubeau F, et al. Texture analysis and morphological processing of magnetic resonance imaging assist detection of focal cortical dysplasia in extratemporal partial epilepsy. Ann Neurol 2001; 49:770–5.
[32] Antel SB, Bernasconi A, Bernasconi N, Collins DL, Kearney RE, Shinghal R, et al. Computational models of MRI characteristics of focal cortical dysplasia improve lesion detection. Neuroimage 2002;17:1755–60.
[33] Bernasconi A, Bernasconi N, Bernhardt BC, Schrader D. Advances in MRI for 'cryptogenic' epilepsies. Nat Rev Neurol 2011;7(2):99–108.
[34] McDonald CR, Hagler Jr DJ, Ahmadi ME, Tecoma E, Iragui V, Gharapetian L, et al. Regional neocortical thinning in mesial temporal lobe epilepsy. Epilepsia 2008;49: 794–803.
[35] Bernhardt BC, Worsley KJ, Besson P, Concha L, Lerch JP, Evans AC, et al. Mapping limbic network organization in temporal lobe epilepsy using morphometric correlations: insights on the relation between mesiotemporal connectivity and cortical atrophy. Neuroimage 2008;42(2):515–24.
[36] Mueller SG, Laxer KD, Barakos J, Cheong I, Garcia P, Weiner MW. Widespread neocortical abnormalities in temporal lobe epilepsy with and without mesial sclerosis. Neuroimage 2009;46(2):353–9.
[37] Labate A, Cerasa A, Aguglia U, Mumoli L, Quattrone A, Gambardella A. Neocortical thinning in "benign" mesial temporal lobe epilepsy. Epilepsia 2011;52(4):712–7.
[38] Fauser S, Sisodiya SM, Martinian L, Thom M, Gumbinger C, Huppertz HJ, et al. Multifocal occurrence of cortical dysplasia in epilepsy patients. Brain 2009;132:2079–90.
[39] Wallace BC, Small K, Brodley CE, Trikalinos TA. Class imbalance, redux. Proc IEEE Int Conf Data Mining 2011:754–63.
[40] Bishop CM. Pattern recognition and machine learning. New York: Springer-Verlag; 2006.
[41] Antel SB, Collins DL, Bernasconi N, Andermann F, Shinghal R, Kearney RE, et al. Automated detection of focal cortical dysplasia lesions using computational models of their MRI characteristics and texture analysis. Neuroimage 2003;19(4):1748–59.
[42] Dice LR. Measures of the amount of ecologic association between species. Ecology 1945;26(3):297–302.
[43] Zijdenbos AP, Dawant BM, Margolin RA, Palmer AC. Morphometric analysis of white matter lesions in MR images: method and validation. IEEE Tran Med Imag 1994; 13(4):716–24.
[44] Zou KH, Warfield SK, Bharatha A, Tempany CM, Kaus MR, Haker SJ, et al. Statistical validation of image segmentation quality based on a spatial overlap index. Acad Radiol 2004;11(2):178–89.
[45] Babalola KO, Patenaude B, Aljabar P, Schnabel J, Kennedy D, Crum W, et al. Comparison and evaluation of segmentation techniques for subcortical structures brain MRI. Med Image Comput Comput Assist Interv 2008;11(Pt 1):409–16.
[46] Blumcke I, Spreafico. Cause matters: a neuropathological challenge to human epilepsies. Brain Pathol 2012;22:347–9.
[47] Sisodiya SM. Surgery for malformations of cortical development causing epilepsy. Brain 2000;123(6):1075–91.
[48] Sisodiya SM. Surgery for focal cortical dysplasia. Brain 2004;127(11):2383–4.
[49] Bell ML, Rao S, So EL, Trenerry M, Kazemi N, Stead SM, et al. Epilepsy surgery outcomes in temporal lobe epilepsy with a normal MRI. Epilepsia 2009;50(9):2053–60.
[50] Garbelli R, Milesi G, Medici V, Villani F, Didato G, Deleo F. Blurring in patients with temporal lobe epilepsy: clinical, high-field imaging and ultrastructural study. Brain 2012;135:2337–49.
[51] Casanova MF, El-Baz AS, Kamat SS, Dombroski BA, Khalifa F, Elnakib A, et al. Focal cortical dysplasias in autism spectrum disorders. Acta Neuropathol Commun 2013; 1(1):67.
[52] Blumcke I, Thom M, Aronica E, Armstrong DD, Vinters HV, Palmini A, et al. The clinicopathologic spectrum of focal cortical dysplasias: a consensus classification proposed by an ad hoc Task Force of the ILAE Diagnostic Methods Commission. Epilepsia 2011;52(1):158–74.